

# An Innovative miR-Activated Scaffold for the Delivery of a miR-221 Inhibitor to Enhance Cartilage Defect Repair

Claudio Intini, Lia Blokpoel Ferreras, Sarah Casey, James E. Dixon, John P. Gleeson, and Fergal J. O'Brien\*

The development of treatments to restore damaged cartilage that can provide functional recovery with minimal risk of revision surgery remains an unmet clinical need. Gene therapy shows increased promise as an innovative solution for enhanced tissue repair. Within this study a novel microRNA (miR)-activated scaffold is developed for enhanced mesenchymal stem/stromal cells (MSC) chondrogenesis and cartilage repair through the delivery of an inhibitor to microRNA-221 (miR-221), which is known to have a negative effect of chondrogenesis. To fabricate the miR-activated scaffolds, composite type II collagen-containing scaffolds designed specifically for cartilage repair are first manufactured by lyophilization and then functionalized with glycosaminoglycan-binding enhanced transduction (GET) system nanoparticles (NPs) encapsulating the miR-221 inhibitor. Subsequently, scaffolds are cultured with human-derived MSCs *in vitro* under chondrogenic conditions for 28 days. The miR-activated scaffolds successfully transfect human MSCs with the miR-221 cargo in a sustained and controlled manner up to 28 days. The silencing of miR-221 in human MSCs using the miR-activated scaffold promotes an improved and more robust cell-mediated chondrogenic response with repressed early-stage events related to MSC hypertrophy. Taken together, this innovative miR-activated scaffold for the delivery of a miR-221 inhibitor demonstrates capability to improve chondrogenesis with promise to enhance cartilage defect repair.

highly porous type I/II collagen-hyaluronic acid (CI/II-HyA) scaffold have proved to be effective in enhancing early cartilaginous matrix deposition while also providing a regenerative template for new tissue formation *in vivo*.<sup>[4–7]</sup> However, when developing a scaffold biomaterial for cartilage repair, it is crucial to consider that a mesenchymal stem/stromal cell (MSC) population, already inclined toward an osteogenic lineage via hypertrophic differentiation, may colonize the implant, subsequently leading to aberrant calcified cartilage formation.<sup>[8–10]</sup> Accordingly, the development of a biomaterial capable of effecting greater control on the MSC chondrogenic differentiation process is likely to offer more potent treatments for cartilage-related pathologies.<sup>[11,12]</sup> To this end, advanced biomaterials capable of directing sustained and controlled MSC differentiation, through the incorporation of nonviral nanoparticles (NPs) for the delivery of therapeutic genes, have been developed in our laboratory.<sup>[13–17]</sup> Specifically, these advanced biomaterials (termed gene-activated scaffold platforms) have successfully directed MSC transfection using non-viral vectors for enhanced bone and cartilage repair.<sup>[13,18–20]</sup>

One of these NPs, a nonviral peptide-based delivery system termed glycosaminoglycan (GAG)-binding enhanced transduction (GET), has been exploited in advanced biomaterials for

## 1. Introduction

Biomaterials offer some promise to fully restore articular cartilage defects.<sup>[1–3]</sup> For example, biomimetic biomaterials such as a

C. Intini, L. B. Ferreras, S. Casey, F. J. O'Brien  
Tissue Engineering Research Group  
Department of Anatomy and Regenerative Medicine  
Royal College of Surgeons in Ireland (RCSI) University of Medicine and Health Sciences  
Dublin D02 YN77, Ireland  
E-mail: fjobrien@rcsi.ie

 The ORCID identification number(s) for the author(s) of this article can be found under <https://doi.org/10.1002/adtp.202200329>

© 2023 The Authors. Advanced Therapeutics published by Wiley-VCH GmbH. This is an open access article under the terms of the Creative Commons Attribution-NonCommercial-NoDerivs License, which permits use and distribution in any medium, provided the original work is properly cited, the use is non-commercial and no modifications or adaptations are made.

DOI: 10.1002/adtp.202200329

C. Intini, L. B. Ferreras, S. Casey, F. J. O'Brien  
Advanced Materials and Bioengineering Research (AMBER) Centre  
RCSI and TCD  
Dublin D02 CP49, Ireland

J. E. Dixon  
Regenerative Medicine and Cellular Therapies  
School of Pharmacy  
University of Nottingham  
Nottingham NG7 2RD, UK

J. P. Gleeson  
Fraunhofer Project Centre for Embedded Bioanalytical Systems  
Dublin City University, Glasnevin  
Dublin 9, Ireland

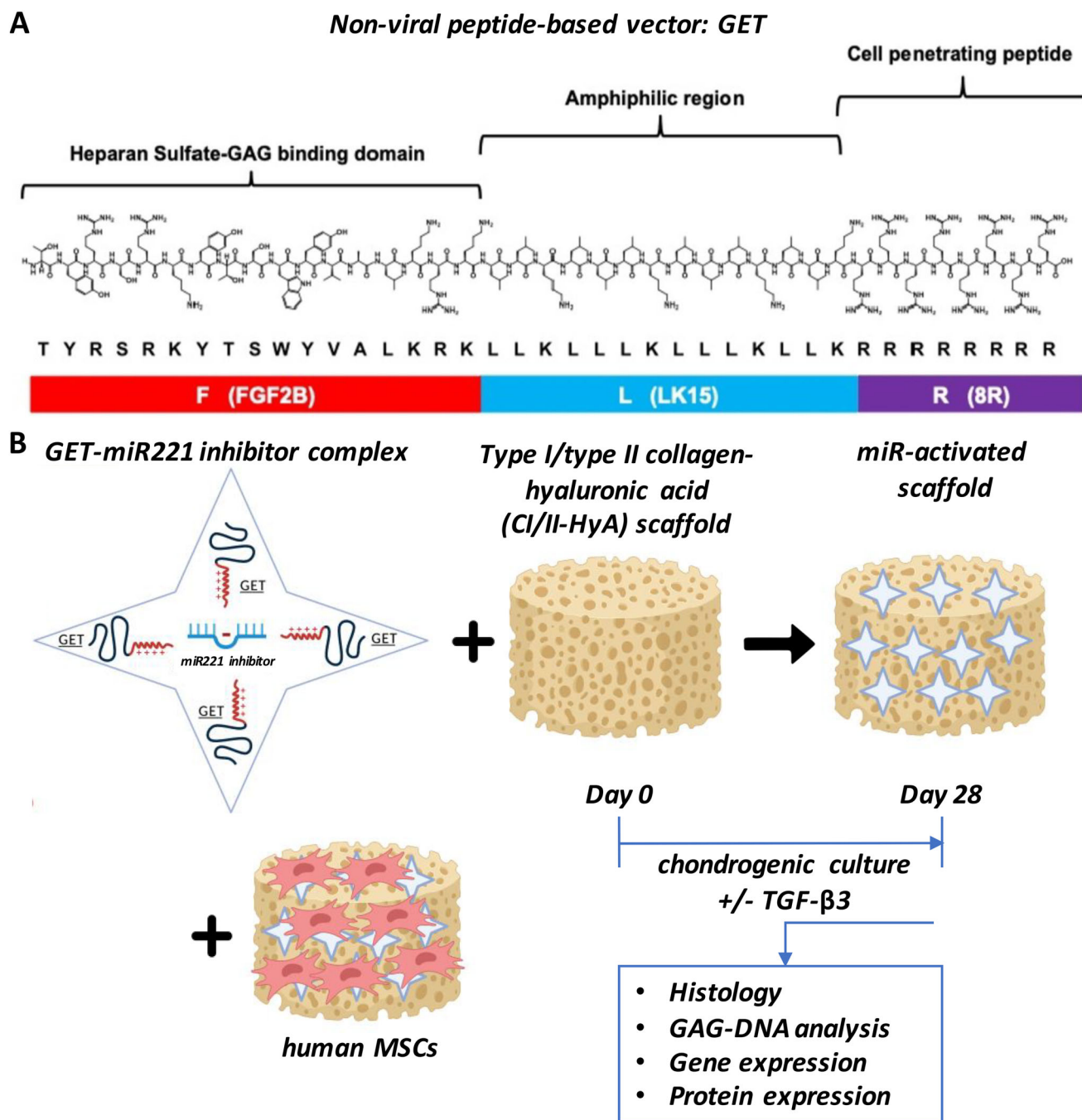


**Figure 1.** Illustrative scheme describing the study design. Representation of GET peptide: A) a glycosaminoglycan (GAG)-binding peptide sequence (P21), fused to an amphiphilic region with an octa-arginine (8R) and a cell-penetrating peptide (CPP).<sup>[15]</sup> B) Illustrative scheme describing the experimental design.

enhanced repair of hard and soft tissues.<sup>[15,21–23]</sup> Specifically, GET is a multidomain peptide comprising a GAG-binding peptide sequence with cell penetrating peptide components (Figure 1A).<sup>[21]</sup> Recently, GET has been shown to transfect genetic cargos such as plasmid DNAs (pDNAs) to several different cell types with high efficiency, and with no impact on cellular cytotoxicity.<sup>[15]</sup> In addition, GET-pDNA activated scaffolds were

proven to be capable of delivering, in a sustained and controlled manner, specific therapeutic pDNAs coding for osteogenic (bone morphogenetic protein-2, BMP-2) and angiogenic (vascular endothelial growth factor, VEGF) proteins for enhanced osteogenesis and the repair of critical sized calvarial bone defect in rats.<sup>[15]</sup> The intra- and extracellular mechanisms governing GET uptake within cellular phenotypes seem to be played by the positively

charged amino acids constituting GET which ensure effective cellular endocytosis and translocation of the genetic cargo in the cell.<sup>[19,24]</sup> Previous studies have proven GET's capability to efficiently transfect rat-derived MSCs with pDNA, resulting in improved bone-like tissue formation in vitro.<sup>[15]</sup> However, GET's capacity to transfect human-derived MSCs (hMSCs) with therapeutic microRNAs (miRNAs) for cartilage repair remains to be elucidated.

The development of advanced biomaterials capable of efficiently delivering microRNA-based therapeutics to MSCs in a sustained and tissue-specific manner is of great interest in the field.<sup>[25–27]</sup> miRNAs are short noncoding RNA molecules, which target specific small interfering RNAs that in turn can regulate the expression of specific genes by silencing protein translation.<sup>[19,28–30]</sup> miRNAs can act as regulators of the differentiation fate of a number of (specific) cell populations by activating or inhibiting entire intracellular pathways.<sup>[30,31]</sup> In this study, microRNA-221 (miR-221) was chosen as a target of interest given its known involvement in the chondrogenic process of MSCs.<sup>[32–34]</sup> Recent researches have revealed the potential of enhanced MSC chondrogenesis and cartilage-like tissue formation in vitro and in vivo models when miR-221 is downregulated.<sup>[32,33,35]</sup> Specifically, it has been hypothesized that miR-221 is involved in reducing the expression of cartilage-fate major factors such as Runt-related transcription factor 2 (*RUNX2*), which is associated with increased hypertrophy and, subsequent calcified cartilage formation.<sup>[33,36]</sup>

Building on this knowledge, the primary hypothesis of this study was that the silencing of miR-221, through the incorporation of GET NPs into CI/II-HyA scaffolds, would positively influence hMSC behavior leading to improved chondrogenesis and cartilage-like tissue formation in vitro. To this end, the specific aims were: 1) to optimize the delivery of a short noncoding RNA molecule, namely, a miR-221 inhibitor, to hMSCs via the GET delivery system in two-dimensional (2D), 2) to develop a miR-221-activated scaffold using the previously designed CI/II-HyA scaffold for cartilage repair, and 3) to assess the effect of miR-221 silencing on MSC chondrogenesis and cartilage-like formation in vitro.

## 2. Experimental Section

### 2.1. Cell Culture

To obtain a sufficient quantity of hMSCs, cells were first expanded in monolayer. MSCs were isolated from the bone-marrow of adults (donor age range: 20–30 years old) (purchased from Lonza (Switzerland) using standard protocols including a stringent analysis of cell phenotype as previously described.<sup>[37]</sup> The cells were incubated with low-glucose Dulbecco's modified Eagle's medium (DMEM) (Sigma-Aldrich, Ireland) supplemented with 10% fetal bovine serum (ThermoFisher Scientific, Ireland) and 1% penicillin/streptomycin (ThermoFisher Scientific, Ireland). Cells were passaged by trypsinization once confluent, and replated onto T-175 (175 cm<sup>2</sup> growth area) flasks under normoxic cell culture conditions (37 °C, 5% CO<sub>2</sub>, 21% O<sub>2</sub>). Cells were cultured in monolayer and on the scaffold at passage number 4 (Figure 1B).

**Table 1.** Experimental miR-activated scaffolds investigated in this study. CI/II-HyA scaffolds composed of type I collagen (CI) and type II collagen (CII) with a final collagen concentration of 0.5% (w/v), in the presence of hyaluronic acid (HyA) at concentration of 0.05% (w/v) were manufactured and adapted as miR-free (MF) and miR-activated (MA) scaffolds in culture, with or without TGF- $\beta$ 3 supplementation.

Experimental group	Nomenclature
miR-free scaffolds	MF
miR-free scaffolds + TGF- $\beta$ 3	MF + TGF- $\beta$ 3
miR-activated scaffolds	MA
miR-activated scaffolds + TGF- $\beta$ 3	MA + TGF- $\beta$ 3

### 2.2. Transfection of Cells with miR-221 Inhibitor

To transfect the cells, the peptide-based nonviral vector, GET (FLR) peptide, was used as previously described.<sup>[15]</sup> Lipofectamine 3000 (ThermoFisher Scientific, Ireland), which represents a commercially available lipid-based nonviral vector, was used as a control. Cells were seeded in monolayer at a density of  $0.2 \times 10^5$  cells per well on tissue culture-treated plastic 24 h prior to transfection. Based on preliminary experimentation carried out in the laboratory, GET NPs at a concentration of 1 mM were added to a hsa-miR-221-3p miRIDIAN antagomiR solution (miR-221 inhibitor) (Horizon discovery, UK) prepared at a final concentration of 40 nM per well, before allowing to complex for 15 min in OptiMEM buffer (ThermoFisher Scientific, Ireland). GET-miR-221 inhibitor complexes at a final volume of 50  $\mu$ L were formulated at a charge ratio (CR) of GET to antagomiR-221-3p of CR 5:1, with the miRNA concentration remaining constant at 40 nM. Cell growth media was changed 1 h prior to transfection at a volume of 500  $\mu$ L per well, and GET-miR-221 inhibitor complex solution was added directly to the media at a volume of 50  $\mu$ L per well. Lipofectamine 3000 (ThermoFisher Scientific, Ireland) was used as a control as per manufacturers recommendations with the miRNA concentration remaining constant at 40 nM. The growth medium was replaced after 24 h, supplemented with the chondrogenic factors +/- 10 ng mL<sup>-1</sup> human transforming growth factor beta-3 (TGF- $\beta$ 3) (Prospec, Israel). This chondrogenic media was composed of serum-free high-glucose DMEM supplemented with 50  $\mu$ g mL<sup>-1</sup> ascorbic acid (Sigma-Aldrich, Ireland), 40  $\mu$ g mL<sup>-1</sup> proline (Sigma-Aldrich, Ireland), 100 nM dexamethasone (Sigma-Aldrich, Ireland), 1 $\times$  ITS (BD Biosciences, UK), and 0.11 mg mL<sup>-1</sup> sodium pyruvate (Sigma-Aldrich, Ireland). The well plates were incubated for 3 and 14 days, with media changed twice per week.

### 2.3. Fabrication of miR-Activated Scaffolds

To fabricate the miR-activated scaffolds, a freeze-drying (lyophilization) method was used, in combination with a cell-transfection protocol previously described in the research group (Table 1).<sup>[15,38]</sup> Briefly, CI/II-HyA scaffolds were manufactured and dehydrothermally crosslinked as previously described.<sup>[5]</sup> Subsequently, GET-miR-221 inhibitor complexes at a final volume of 25  $\mu$ L were formulated at CR 5:1, GET to antagomiR-221 as described in Section 2.2. Following this, the GET-miR-221 inhibitor complex was added to the cell-free scaffolds, with 12.5  $\mu$ L

first pipetted onto one side of each scaffold, before incubating for 15 min (5% CO<sub>2</sub>, 37 °C). Scaffolds were subsequently turned over and the procedure repeated on the other side. Following, the MSCs were detached from their culture flasks via trypsinization. Cells were counted and resuspended at a density of 5 × 10<sup>5</sup> cells per scaffold in a total volume of 100 μL. Scaffolds of 9.5 mm diameter and 4 mm height were prehydrated in phosphate buffered saline (PBS) (Sigma-Aldrich, Ireland) for 15 min and placed in 24-well plates. The cell suspension was then added to the scaffolds, with 50 μL first pipetted onto one side of each scaffold, before incubating for 30 min (37 °C, 5% CO<sub>2</sub>, 21% O<sub>2</sub>) to allow initial cell attachment. Seeded scaffolds were subsequently turned over and the procedure repeated on the other side. After seeding and transfection, 2 mL of expansion/growth medium was added to each well before culturing for 24 h in normoxic conditions. The growth medium was then replaced with medium supplemented with chondrogenic factors +/- 10 ng mL<sup>-1</sup> human TGF-β3 (Prospec, Israel) as described in Section 2.2. The well plates were incubated for 3, 14, and 28 days, with media changed twice per week.

## 2.4. Cellular Metabolic Activity Assay

To determine the cellular metabolic activity of the cells in monolayer and on the scaffold, an AlamarBlue assay (ThermoFisher Scientific, Ireland) was performed. Scaffolds were washed in PBS twice and fresh chondrogenic media containing 10% AlamarBlue viability reagent was added at 37 °C for 1 h. A spectrophotometer (Wallac 1420 Victor2 D, USA) with an excitation wavelength of 550 nm and an emission wavelength of 590 nm was used to read the resulting fluorescence level. Chondrogenic media containing 10% AlamarBlue was used as a blank sample, subtracted from the experimental readings to eliminate background fluorescence. Cellular metabolic activity in monolayer was measured at day 0, 3, 7, and 14 of culture; cell metabolic activity was measured in the cell seeded scaffolds at day 0, 3, 10, 14, and 28.

## 2.5. Gene Expression Analysis

To determine the gene expression levels of miR-221 after transfecting the cells with miR-221 inhibitor, a quantitative real-time polymerase chain reaction (qRT-PCR) was conducted. miR-221 gene expression in monolayer was measured at day 3 and 14 of culture; miR-221 gene expression in the cell seeded scaffolds at day 3, 14, and 28. The total RNA was isolated using a miRNeasy kit (Qiagen, UK) and reverse transcribed to cDNA at the final concentration of 5 ng μL<sup>-1</sup> using a TaqMan Advanced miRNA cDNA Synthesis Kit (ThermoFisher Scientific, Ireland). RT-PCRs were run on a 7500 real-time PCR System (Applied Biosystems, UK) using a TaqMan Fast Advanced Master Mix (ThermoFisher Scientific, Ireland) in combination with a validated TaqMan Advanced miRNA primer for hsa-miR-221-3p (ThermoFisher Scientific, Ireland). Furthermore, the gene expression levels of specific markers associated with chondrogenic lineage were determined in the cell seeded scaffolds at day 3, 14, and 28. The total RNA previously isolated was reverse transcribed to cDNA at a final concentration of 2.5 ng μL<sup>-1</sup> using a QuantiTect reverse-transcription kit (Qiagen, UK) and run on the 7500 real-time

PCR system. The relative expression of mRNA was calculated by delta-delta Ct (ΔΔCt) method. The expression of hsa-miR-221-3p (miR-221), aggrecan (*ACAN*), type II collagen alpha 1 chain (*COL2A1*), matrix metalloproteinase-13 (*MMP-13*), runt-related transcription factor 2 (*RUNX2*), snail family transcriptional repressor 1 (*SNAI1*), and transcriptional repressor GATA binding 1 (*TRPS1*) was analyzed (Table 2). Glyceraldehyde 3-phosphate dehydrogenase (*GAPDH*) and 18S ribosomal RNA (*18S*) were used as housekeeping genes.

## 2.6. Protein Expression Analysis

To determine the level of protein expression of RUNX-2, a specific protein typically associated with early-stage hypertrophic events and calcified cartilage, western blotting analysis was conducted at day 28.<sup>[39]</sup> Cell seeded scaffolds were manually homogenized, followed by measurement of the total protein content using a Pierce BCA Protein Assay Kit (ThermoFisher Scientific, Ireland). 10 μg total protein was separated by electrophoresis and subsequently transferred to a polyvinylidene fluoride or polyvinylidene difluoride membrane (Sigma-Aldrich, Ireland). The membrane was incubated at 4 °C overnight with 1:1000 diluted rabbit polyclonal anti-RUNX-2 (RUNX-2) antibody (Abcam, ab23981) and 1:5000 rabbit polyclonal anti-GAPDH (GAPDH) antibody (Abcam, ab9485). Membranes were washed and then incubated with the respective secondary antibody for 1 h at room temperature (1:5000). Protein bands were visualized using the Super Signal West detection kit (Thermo Fisher Scientific, Ireland). Protein bands were quantified using ImageJ2 software version 2.3.0.

## 2.7. DNA Quantification

To assess the DNA content per scaffold, a Quant-iT PicoGreen ds-DNA assay kit (Invitrogen, UK) was used as per manufacturer's instructions. Scaffolds were washed in PBS and digested in a papain enzyme solution prepared with 0.5 M EDTA, cysteine-HCl and 1 mg mL<sup>-1</sup> papain enzyme (Carica papaya, Sigma-Aldrich, Ireland) at 60 °C for 12 h. DNA concentration was determined using a standard curve, to give an indication of cell number. DNA content was measured in the cell seeded scaffolds at day 28. The DNA quantified on the scaffolds was also tested for cellular metabolic activity.

## 2.8. Sulfated Glycosaminoglycan (sGAG) Quantification

To quantify the sGAG content per scaffold, a Blyscan sulfated glycosaminoglycan assay kit (Biocolor Life Sciences, UK) was used as per the manufacturer's instructions. Scaffolds were washed in PBS before digesting as described in Section 2.7. sGAG content was determined using a standard curve and was measured in the cell seeded scaffolds at day 28.

## 2.9. Histological Analysis of Cellular Infiltration and sGAG Distribution

To reveal cellular infiltration and negatively charged sGAG distribution in the scaffolds, histological staining was performed

**Table 2.** List of gene transcripts analyzed by qRT-PCR. Qiagen QuantiTect validated primers used to analyze the expression levels of target genes.

Target gene	Target gene reference	Catalogue code
Aggrecan (ACAN)	Hs_ACAN_1_SG	QT00001365
Type II collagen alpha 1 chain (COL2A1)	Hs_COL2A1_1_SG	QT00049518
Matrix metalloproteinase-13 (MMP-13)	Hs_MMP13_1_SG	QT00001764
Runt-related transcription factor 2 (RUNX2)	Hs_RUNX2_1_SG	QT00020517
Snail family transcriptional repressor 1 (SNAI1)	Hs_SNAI1_1_SG	QT00010010
Transcriptional repressor GATA binding 1 (TRPS1)	Hs_TRPS1_1_SG	QT00035763
Glyceraldehyde 3-phosphate dehydrogenase (GAPDH)	Hs_GAPDH_1_SG	QT00079247
18S ribosomal RNA (18S)	Hs_RRN18S_1_SG	QT00199367

at day 28. Scaffolds were formalin-fixed, paraffin-embedded, and transversally sectioned at various depths on a microtome (Leica RM 2255, Leica, Germany) to give 7  $\mu\text{m}$  thick sections. These sections were subsequently mounted on Polysine glass slides (Fisher-Scientific, Ireland), deparaffinized and hydrated before staining. Stains used in the histological analysis were hematoxylin (Sigma-Aldrich, Ireland), which stains the DNA- and RNA-rich cell nuclei blue, eosin (Sigma-Aldrich, Ireland), which stains the extracellular matrix pink, and thionine (Sigma-Aldrich, Ireland), which stains negatively charged sGAG purple.<sup>[40,41]</sup>

### 2.10. Statistical Analysis

Results are expressed as mean  $\pm$  standard deviation unless otherwise stated. Statistical analysis was performed using GraphPad Prism software version 9.2.0 using a general linear model ANOVA with Fisher's LSD test analysis performed for multiple comparisons.  $p$ -values less than or equal to 0.05 ( $p < 0.05$ ) were considered statistically significant. \* denotes  $p < 0.05$ , \*\* =  $p < 0.01$ , \*\*\* =  $p < 0.001$ , and \*\*\*\* =  $p < 0.0001$ .

## 3. Results

### 3.1. GET NPs Facilitated the Delivery of miR-221 Inhibitor to hMSCs with No Impact on Cellular Metabolic Activity

To assess delivery efficiency and biocompatibility, the capability of GET NPs to deliver the miR-221 inhibitor to hMSCs without affecting cellular metabolic activity was investigated and compared with that of Lipofectamine 3000 (which represents a commercially available lipid-based nonviral vector, regularly used as control).<sup>[15]</sup> Gene expression levels of *miR-221* in cells grown in 2D +/- TGF- $\beta$ 3 and transfected with GET- or Lipofectamine-miR-221 inhibitor NPs (miR-activated, MA) were measured at day 3 and 14 and compared to miR-free cells (MF). The delivery of GET-miR-221 inhibitor NPs to MA cells +/- TGF- $\beta$ 3 reduced *miR-221* expression at day 3 and 14 compared to MF cells +/- TGF- $\beta$ 3 (Figure 2D). Additionally, the delivery of GET NPs had no impact on the metabolic activity of the cells (Figure 2C). Specifically, at day 0, 3, 7, and 14 there was no statistical difference in cellular metabolic activity between groups. However, all cells (transfected or not) showed a significant increase in cellular metabolic activity at day 3 compared to days 0, 7, and 14. Similar results were observed when the GET NPs delivery system

was compared with that of Lipofectamine NPs. The delivery of Lipofectamine-miR-221 inhibitor NPs to MA cells reduced *miR-221* levels at day 3 and day 14 compared to MF cells in the absence of TGF- $\beta$ 3 (Figure 2B). Moreover, similarly to GET NPs, the delivery of Lipofectamine NPs had no impact on cell metabolic activity (Figure 2A). However, in contrast to GET NPs, the delivery of Lipofectamine NPs to MA + TGF- $\beta$ 3 resulted in reduced *miR-221* at day 3 with no significant impact at day 14 compared to MF + TGF- $\beta$ 3 cells.

### 3.2. miR-221 Inhibitor Incorporation into the CI/II-HyA Scaffolds Reduced the Expression of miR-221 by hMSCs

Having confirmed the efficacy of the GET delivery system for hMSC transfection in 2D, its capability to efficiently deliver miR-221 inhibitor to hMSCs when incorporated in CI/II-HyA scaffolds was investigated. Expression levels of *miR-221* by cells grown on miR-activated (MA) scaffolds was measured at day 3, 14, and 28, and compared to miR-free (MF) scaffolds (Figure 3). Furthermore, the effect of TGF- $\beta$ 3 supplementation was investigated. Thus, four groups were investigated as described in Table 1. Gene expression analysis revealed that *miR-221* levels were significantly reduced at day 3, 14, and 28 in MA scaffolds +/- TGF- $\beta$ 3, compared to MF scaffolds +/- TGF- $\beta$ 3 demonstrating that the incorporation of miR-221 inhibitor into CI/II-HyA scaffolds effectively silenced miR-221 expression in a sustained and controlled manner up to day 28 (Figure 3).

### 3.3. miR-221 Silencing Had No Impact on hMSC Viability

To assess biocompatibility, the effect of miR-221 silencing on hMSC viability and growth in culture was evaluated. Biochemical assays revealed that all groups performed well, with an equal ability to sustain cellular viability in scaffolds up to day 28 (Figure 4). The delivery of miR-221 inhibitor had no impact on the metabolic activity of the cells (Figure 4A). Specifically, at days 0, 3, 10, 14, and 28 there was no statistical difference in cellular metabolic activity between MF and MA groups. However, full analysis demonstrated that cells cultured on MF and MA scaffolds in the absence of TGF- $\beta$ 3 had significantly higher levels of metabolic activity at day 14 compared to day 0 (Figure 4A). Additionally, the silencing of *miR-221* had no effect on DNA levels at day 28 (Figure 4B).

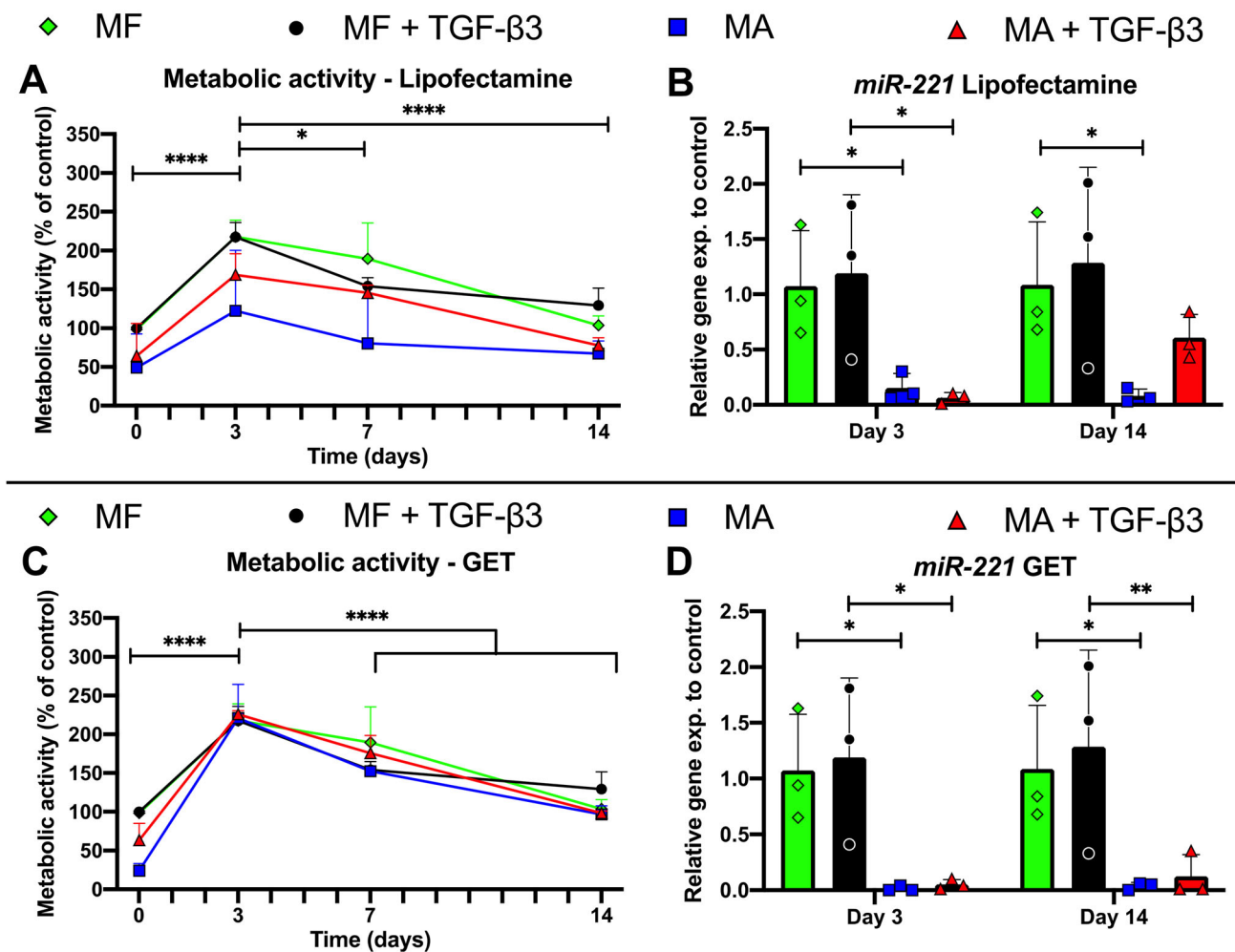


**Figure 2.** The delivery of GET NPs to hMSCs reduced *miR-221* expression with no impact on cellular metabolic activity. Cellular metabolic activity and gene expression of *miR-221* were determined using A,B) Lipofectamine and C,D) GET delivery systems. Cellular metabolic activity was determined and normalized to MF + TGF-β3 at time 0 after 0, 3, 7, and 14 days in culture +/– TGF-β3 supplementation (A,C). Gene expression of *miR-221* was determined after 3 and 14 days in culture +/– TGF-β3 supplementation, normalized to *GAPDH* and then converted to a fold increase in expression using the formula: Fold increase =  $2^{-\Delta\Delta Ct}$ . The amount of target mRNA relative to MA and MA + TGF-β3, was normalized to a calibrator sample, respectively MF and MF + TGF-β3, to generate  $\Delta\Delta Ct$  (B,D). Data presented as mean  $\pm$  SD,  $n = 3$ . \* denotes  $p < 0.05$ , \*\* =  $p < 0.01$ , \*\*\* =  $p < 0.001$ , and \*\*\*\* =  $p < 0.0001$ .

### 3.4. miR-221 Silencing in Combination with TGF-β3 Showed Potential to Direct Improved Chondrogenesis

Further analysis of the effect of miR-221 silencing on hMSC chondrogenic differentiation was then investigated by measuring the expression of specific genetic markers typically associated with effective MSC chondrogenesis and late-stage differentiation.<sup>[39,42]</sup>

All groups showed *ACAN* and *COL2A1* gene expression by the hMSCs (Figure 5A,B). The silencing of miR-221 in combination with TGF-β3 on the MA scaffolds upregulated *ACAN* expression at day 14 compared to MF ( $p < 0.01$ ), MA ( $p < 0.001$ ) and MF + TGF-β3 ( $p < 0.05$ ) scaffolds (Figure 5A). Additionally, *ACAN* significantly increased between days 3 and 14 in MA + TGF-β3 ( $p < 0.0001$ ) and MF + TGF-β3 ( $p < 0.05$ ) scaffolds. However, in con-

trast to MA + TGF-β3, MF + TGF-β3 showed upregulated *ACAN* at day 28 compared to MF ( $p < 0.05$ ), MA ( $p < 0.01$ ). There was no statistical difference in *COL2A1* expression between groups (Figure 5B).

The expression of late-stage MSC chondrogenic genes associated with early-stage MSC-hypertrophic events (*MMP-13* and *RUNX2*) was then investigated. Interestingly, MF + TGF-β3 showed higher *RUNX2* expression at day 28 in comparison to MA + TGF-β3 ( $p < 0.05$ ) (Figure 5D). Moreover, in contrast to MF + TGF-β3, *RUNX2* was significantly reduced between days 14 and 28 in MA + TGF-β3 ( $p < 0.01$ ) (Figure 5D). There was no statistical difference in *MMP-13* expression at day 28 in MA + TGF-β3 scaffolds, compared to MA and MF groups (Figure 5C). However, in contrast to MA + TGF-β3, MF + TGF-β3 showed upregulated *MMP-13* at day 28 compared to MF and MA groups.

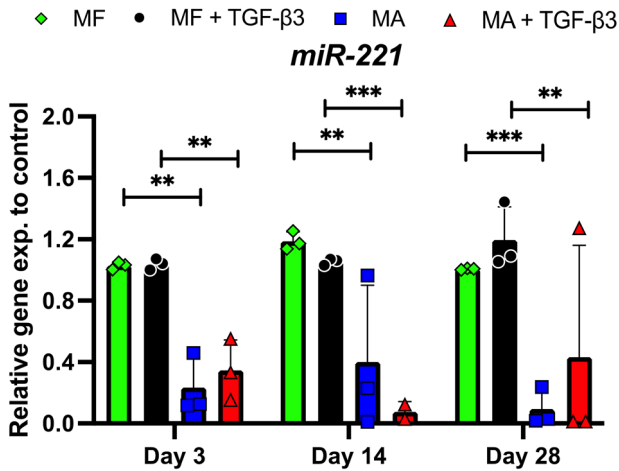


**Figure 3.** The incorporation of miR-221 inhibitor to CI/II-HyA scaffolds reduced the expression of *miR-221* by hMSCs. Gene expression of *miR-221* was determined after 3, 14, and 28 days in culture +/- TGF-β3 supplementation, normalized to *18S* and then converted to a fold increase in expression using the formula: Fold increase =  $2^{-\Delta\Delta Ct}$ . The amount of target mRNA relative to MA and MA + TGF-β3, was normalized to a calibrator sample, respectively MF and MF + TGF-β3, to generate  $\Delta\Delta Ct$ . Data shown represent the average from three individual hMSC donors ( $n = 3$  per donor)  $\pm$  SD. \* denotes  $p < 0.05$ , \*\* =  $p < 0.01$ , \*\*\* =  $p < 0.001$ , and \*\*\*\* =  $p < 0.0001$ .

Furthermore, the expression of cartilage-fate transcriptional factors associated with miR-221's intracellular mechanism of action, *SNAI1* and *TRPS1* genes, was examined.<sup>[32,43,44]</sup> Specifically, high levels of *TRPS1* might inhibit RUNX2-mediated effects on MSC late-stage differentiation and hypertrophy.<sup>[33]</sup> Gene expression analysis revealed that *TRPS1* was significantly upregulated at day 28 in MF + TGF-β3 scaffolds, compared to MF and MA ( $p \leq 0.05$ ) (Figure 5F). However, in contrast to MF + TGF-β3, there was no statistical difference in *TRPS1* in MA + TGF-β3 scaffolds, compared to MF and MA. Overall, there was no statistical differ-

ence in *SNAI1* expression at day 3, 14 or 28 between the groups (Figure 5E).

### 3.5. miR-221 Silencing in Combination with TGF-β3 Decreased RUNX-2 Protein Expression by Day 28

Building on the gene expression results above, the expression of RUNX-2, a key transcription factor protein typically associated with early-stage hypertrophic events and further differentiation to osteogenesis and endochondral bone formation, was analyzed.<sup>[42]</sup> The silencing of miR-221 in the MA + TGF-β3 scaffold decreased the cell-mediated synthesis of RUNX-2 protein by day 28 compared to MF + TGF-β3 (Figure 6). MA + TGF-β3 scaffolds showed less intense stained bands compared to MF + TGF-β3 with seeded scaffolds from donor 1, 2, and 3 (Figure 6). In the absence of TGF-β3, MA scaffolds showed decreased RUNX-2 accumulation per scaffold than MF only with donor 1 and 3 (Figure 6).

### 3.6. miR-221 Silencing Increased MSC-Mediated sGAG Synthesis by Day 28

Further analysis of the effect of miR-221 silencing on cartilage-like matrix formation in vitro was then investigated in the scaffolds. Overall, while the silencing of miR-221 had no impact on the overall sGAG deposition per scaffold (Figure 7A), changes were seen at the cellular level when data were normalized (Figure 7B). Full analysis revealed that the silencing of miR-221 allowed MA + TGF-β3 scaffolds ( $40.11 \mu\text{g mL}^{-1}$ ) to accumulate significantly higher levels of sGAG per cell (sGAG/DNA) compared to MF scaffolds in the absence of TGF-β3 ( $p < 0.05$ ) (Figure 7B). Interestingly, although MF + TGF-β3 scaffolds ( $20.40 \mu\text{g mL}^{-1}$ ) had increased levels of sGAG/DNA compared to MF scaffolds ( $6.63 \mu\text{g mL}^{-1}$ ), this difference was not significant (unlike MA + TGF-β3) (Figure 7B). Moreover, in the absence of TGF-β3, MA

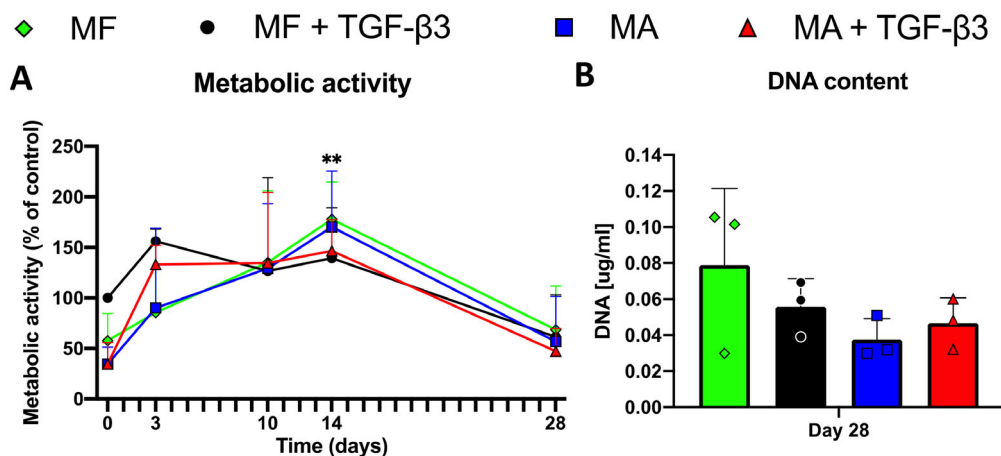


**Figure 4.** The silencing of miR-221 had no impact on hMSC viability. A) Cellular metabolic activity per scaffold was determined and normalized to MF + TGF-β3 scaffolds at time 0 after 0, 3, 10, 14, and 28 days in culture +/- TGF-β3 supplementation. B) DNA content per scaffold was determined after 28 days in culture +/- TGF-β3 supplementation. Data shown represent the average from three individual hMSC donors ( $n = 3$  per donor)  $\pm$  SD. \* denotes  $p < 0.05$ , \*\* =  $p < 0.01$ , \*\*\* =  $p < 0.001$ , and \*\*\*\* =  $p < 0.0001$ .

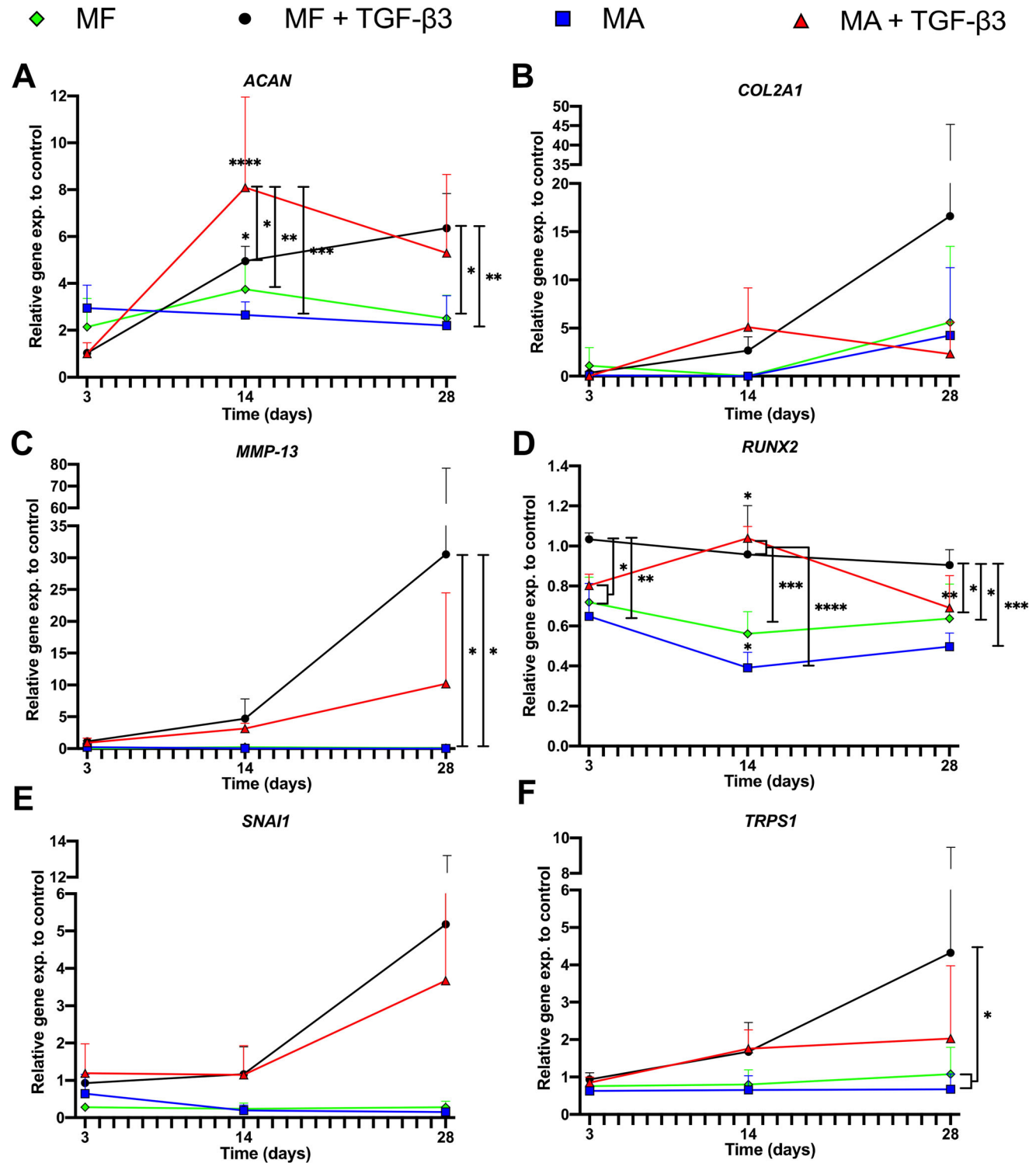


**Figure 5.** The silencing of miR-221 in combination with TGF-β3 showed potential to direct improved MSC chondrogenic differentiation. The gene expression of A) *ACAN*, B) *COL2A1*, C) *MMP-13*, D) *RUNX2*, E) *SNAI1*, and F) *TRPS1* was determined after 3, 14, and 28 days in culture +/– TGF-β3 supplementation, normalized to *18S*, then converted to fold increase in expression using the formula: Fold increase =  $2^{-(\Delta\Delta Ct)}$ . The amount of target mRNA was normalized to MF + TGF-β3 as calibrator sample to generate  $\Delta\Delta Ct$ . Data shown represent the average from three individual hMSC donors ( $n = 3$  per donor)  $\pm$  SD. \* denotes  $p < 0.05$ , \*\* =  $p < 0.01$ , \*\*\* =  $p < 0.001$ , and \*\*\*\* =  $p < 0.0001$ .

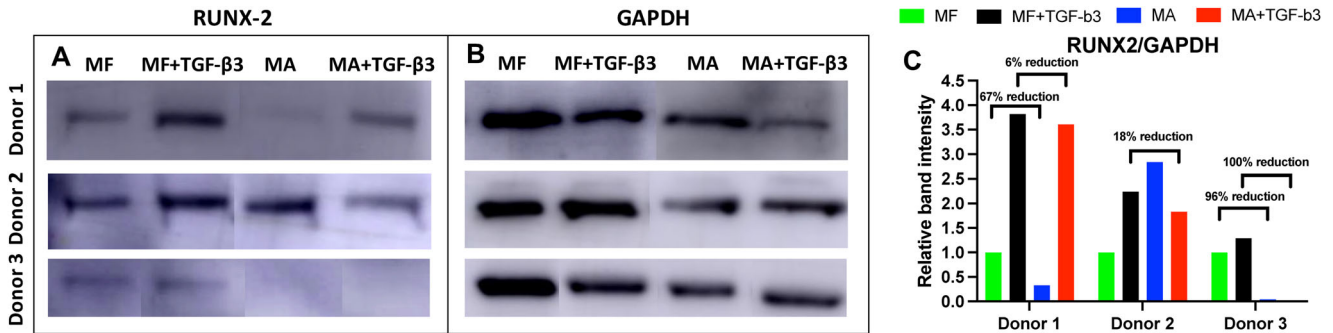


**Figure 6.** The silencing of miR-221 in combination with TGF-β3 directed a cell-mediated decrease in the synthesis of RUNX-2 per scaffold by day 28. The expression of A) RUNX-2 and B) GAPDH (housekeeper) proteins was determined for scaffolds seeded with three individual hMSC donors after 28 days in culture +/- TGF-β3 supplementation. C) The relative protein-band intensity of RUNX-2 was quantified and normalized to GAPDH.

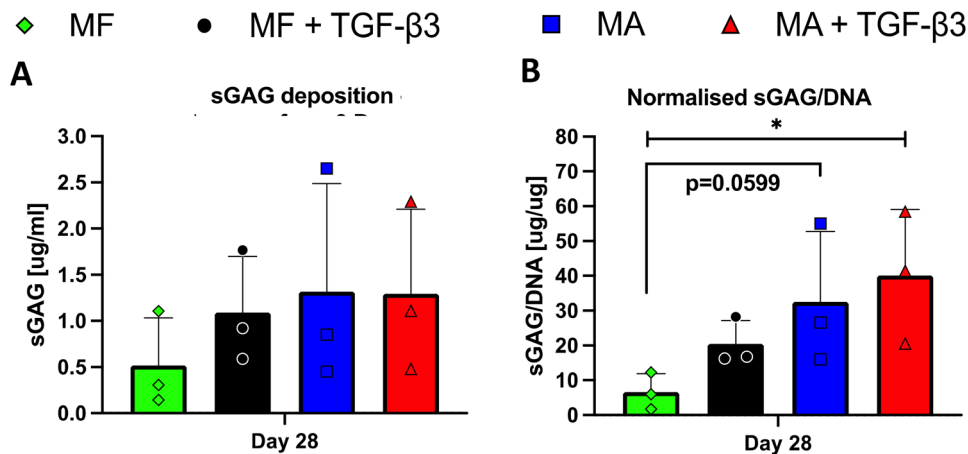


**Figure 7.** The silencing of miR-221 increased MSC-mediated sGAG synthesis at day 28. Overall A) sGAG per scaffold and B) sGAG normalized to DNA content, respectively, were determined after 28 days in culture +/- TGF-β3 supplementation. Data shown represent the average from three individual hMSC donors ( $n = 3$  per donor)  $\pm$  SD. \* denotes  $p < 0.05$ , \*\* =  $p < 0.01$ , \*\*\* =  $p < 0.001$ , and \*\*\*\* =  $p < 0.0001$ .

scaffolds ( $32.56 \mu\text{g mL}^{-1}$ ) resulted in higher levels of sGAG/DNA compared to MF to levels approaching statistical significance ( $p = 0.0599$ ) (Figure 7D).

### 3.7. miR-221 Silencing, in Combination with TGF-β3, Improved sGAG Matrix Distribution

To qualitatively assess the role played by miR-221 silencing on hMSC migration and matrix formation/distribution (represented by the deposition of negatively charged sGAG), histological analysis of the cultured scaffolds was performed. Hematoxylin and eosin staining revealed an equal capability between the groups to direct efficacious cellular infiltration throughout the matrices (Figure 8A). However, miR-221 silencing in the presence of TGF-β3 allowed MA + TGF-β3 scaffolds to achieve more homogeneous sGAG distribution throughout the matrix compared to the other groups as shown by thionine staining (Figure 8B). Interestingly, MA scaffolds in the absence of TGF-β3 performed similarly to MF scaffolds in the presence of TGF-β3. In the absence of TGF-β3, MF scaffolds generally showed minimal evidence of sGAG in the matrices.

## 4. Discussion

The overall aim of this study was to develop a novel miR-activated scaffold for enhanced mesenchymal stem cell mediated chondrogenesis and cartilage repair through the delivery of a miR-221 inhibitor via the GET NPs nonviral delivery system, using a composite CI/II-HyA scaffold designed specifically for cartilage repair.<sup>[4,5]</sup> Specifically, miR-221 was chosen in this study as a target of interest given its potential for enhanced MSC chondrogenesis and cartilage-like formation when downregulated.<sup>[32,33]</sup> To this end, the delivery of the miR-221 inhibitor to hMSCs was first optimized in 2D using the GET peptide. Then, GET was demonstrated to be a suitable carrier for hMSC transfection with the miR-221 inhibitor when incorporated into the previously developed CI/II-HyA 3D scaffold cartilage repair platform.<sup>[4,5]</sup> Specifically, the newly designed miR-221-activated scaffold facilitated effective inhibition of miR-221 up to 28 days with no impact on cellular viability. The silencing of miR-221 in the presence of TGF-β3, a potent chondrogenic factor, demonstrated potential to further improve MSC chondrogenesis with up-regulated ACAN (a principal cartilage ECM component) expression at day 14 and reduced deposition of RUNX-2 (a key transcriptional factor associated with early-stage MSCs hypertrophic events and en-

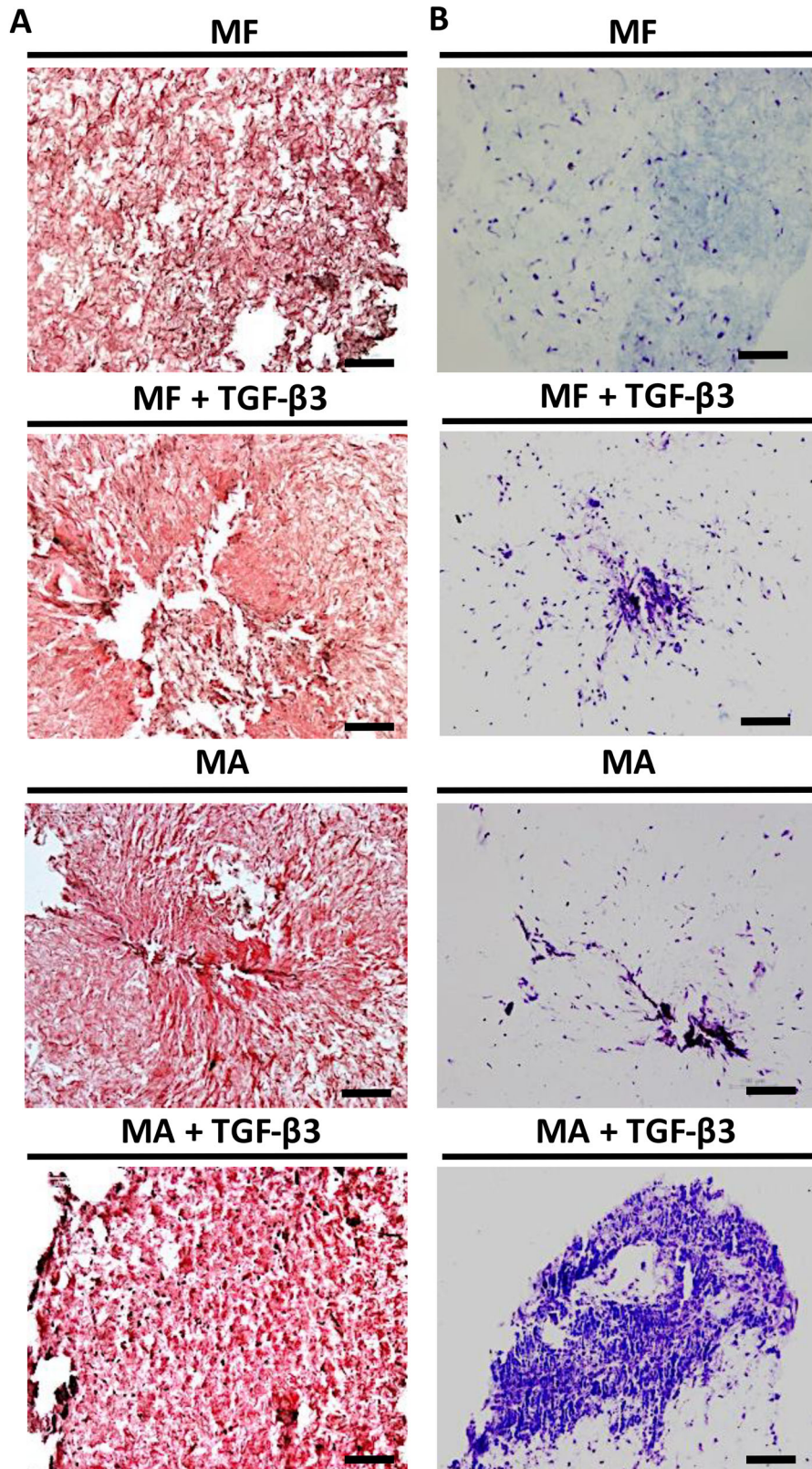


**Figure 8.** The silencing of miR-221 in combination with TGF- $\beta$ 3 improved sGAG distribution. Representative histological images of cell-seeded scaffolds stained with A) hematoxylin and eosin and B) thionine after 28 days in culture +/- TGF- $\beta$ 3 supplementation. Scale bars represent 100  $\mu$ m length.

dochondral bone formation) protein by day 28. Additionally, in the presence of TGF- $\beta$ 3, the miR-221-activated scaffolds demonstrated improved deposition and distribution of cartilage-like tissue in vitro showing the potential of the novel platform as a strategy for enhanced cartilage repair.

Full analysis in 2D revealed that the GET delivery system was a suitable and biocompatible carrier for human MSC transfection and comparable to the commercially available Lipofectamine 3000. Specifically, GET facilitated effective intracellular delivery of the novel therapeutic miR-221 inhibitor into hMSCs with no impact on cellular metabolic activity. These results are not unexpected, and reflect recent research which has shown that GET is a highly versatile delivery system for several genetic cargos such as pDNAs.<sup>[15]</sup> However, this was the first demonstration of the ability of this nonviral delivery system to successfully deliver a miRNA genetic cargo to hMSCs cultured in a sustained and controlled manner up to 14 days in vitro. Taken together, this result opened up the possibility for development of a miR-activated scaffold for cartilage repair through the incorporation of GET NPs for the delivery of specific miRNAs/miR modulators.

Subsequently, the capability of the GET delivery system to act as a microRNA carrier in a 3D scaffold platform was also investigated. Incorporation of GET NPs into the optimized CI/II-HyA scaffold platform for cartilage repair demonstrated successful transfection of hMSCs with the miRNA cargo in a sustained and controlled manner up to 28 days in vitro. The expression levels of *miR-221* by the hMSCs were significantly reduced at days 3, 14, and 28 in the presence of scaffolds incorporating GET NPs with the miR-221 inhibitor demonstrating the efficacy of this miR-activated scaffold system. While this is a breakthrough for cartilage repair, we have previously developed a similar in concept miR-activated scaffold system for bone repair, capable of delivering miRNA therapeutics through the incorporation of an alternative nonviral delivery system utilizing nanohydroxyapatite (n-HA) NPs.<sup>[18,45]</sup> However, n-HA NPs possess the ability to act as bioactive biomaterial, specifically promoting improved cellular responses toward bone-like tissue formation, when incorporated in collagen-based repair platforms.<sup>[46–49]</sup> Therefore, these bone-specific scaffold systems utilizing n-HA NPs are not suitable for our purposes to control enhanced MSC chondrogenesis with limited hypertrophy and, subsequent bone formation. As a result, the newly miR-activated scaffold described in this study offers promise to be a more versatile biomaterial capable to be utilized specifically for cartilage repair and in a number “off the shelf” tissue repair applications through the delivery of therapeutic miRNAs via GET peptide.

Following effective miR-221 silencing, the miR-activated scaffold promoted an improved and more robust MSC-mediated chondrogenic response with effective potential to repress early-stage events related to MSC hypertrophy. Specifically, miR-221 silencing in hMSCs, in the presence of TGF- $\beta$ 3, was shown to reduce the expression of RUNX-2 by day 28 in both gene and protein expression analyses. RUNX-2 is a key transcriptional factor associated with early-stage chondrocyte hypertrophic differentiation and subsequent endochondral bone formation.<sup>[39,42]</sup> While there are no current studies to corroborate these findings directly, previous studies have postulated an indirect effect played by miR-221 in hMSCs on RUNX-2 expression and subsequent downstream hypertrophy-related factors.<sup>[33,36]</sup> Specifically, it has been

reported that the silencing of miR-221 in hMSCs in the absence of exogenous growth factors can lead to repressed RUNX-2 function via TRPS1 (a transcriptional factor regulator of MSC chondrogenic differentiation) levels.<sup>[32,43]</sup> With this in mind, although the results in this study supported the hypothesis that miR-221 has an effect on RUNX-2 expression of the cells, it did not demonstrate a clear effect of miR-221 silencing on *TRPS1* gene expression. To this end, further research is needed to better comprehend miR-221's intracellular mechanism of action during MSC chondrogenic differentiation.

Additionally, the silencing of miR-221 in hMSCs using the miR-activated scaffold promoted an improved and more sustained hMSC-mediated chondrogenic response. In particular, the silencing of miR-221 in the presence of TGF- $\beta$ 3 significantly upregulated *ACAN* expression at day 14 compared to the other groups. These findings are in agreement with what has been hypothesized by other studies which report that high cellular levels of miR-221 can have an indirect inhibitory effect on *ACAN* gene expression.<sup>[33]</sup> Furthermore, our results have proven the potential for the miR-activated scaffold to promote improved deposition and distribution of cartilage-like tissue in vitro. In particular, miR-221 silencing in combination with TGF- $\beta$ 3 resulted in significantly enhanced cartilage-like matrix deposition (normalized to sGAG/DNA) compared to miR-free (MF) scaffolds in the absence of TGF- $\beta$ 3. In this context, although MF + TGF- $\beta$ 3 scaffolds had higher sGAG/DNA levels than MF scaffolds, the difference was not significant as seen in comparison with MA + TGF- $\beta$ 3 scaffolds. Therefore, the results indicated enhanced MSC-mediated cartilage-like deposition due to miR-221 silencing. Similar results were observed by a previous study that intracellularly silenced miR-221 in hMSCs (using Lipofectamine as the nonviral vector) cultivated in 3D pellet systems up to 21 days.<sup>[32,33]</sup> Furthermore, a beneficial chondrogenic effect of miR-221 silencing in hMSCs was illustrated using miR-221 treated cells seeded on an alginate-based gel by 12 weeks postimplantation in rats.<sup>[33]</sup> However, despite the positive results achieved using this alginate-based gel in vivo, this system relies on the need to pretreat the cells in advance with a miR-221 inhibitor prior to implantation. From a clinical perspective, this may represent a limitation in the application of this biomaterial for the treatment of focal cartilage defects.<sup>[19]</sup> Contrastingly, the approach presented in this study has led to the development of a miR-221 activated scaffold designed specifically for cartilage repair, which offers a prospective and promising “off the shelf” approach, capable of directing repair by host cells while also providing a regenerative template for new tissue formation. It can thus potentially be utilized as a minimally invasive single stage surgical procedure to enhance repair of cartilage damage. Taken together, these results interestingly indicate a potential for the miR-activated scaffolds in controlling a more effective MSC chondrogenesis, consequently promoting increased quantity and quality of the biomimetic engineered tissues with the promise of enhanced repair of cartilage damages.

## 5. Conclusion

This study demonstrates that the incorporation of therapeutic microRNAs into a scaffold designed specifically for cartilage repair might be a promising approach for the treatment of cartilage damage and disease. From a clinical perspective, the approach

presented in this study, which has led to the development of a miR-221 activated scaffold, offers a strong “off the shelf” prospective as a simple therapeutic device to support improved cartilage repair in the clinic by targeting host cells in a minimally invasive single stage surgical procedure. Moreover, this innovative miR-activated scaffold offers promise to be utilized and adapted in a number “off the shelf” applications in other tissues such as for skin or nervous system repair for the delivery of alternative therapeutic miRNAs via the GET peptide.

## Acknowledgements

This work was financially supported by the European Union's Horizon 2020 research and innovation programme under Marie Skłodowska-Curie Grant Agreement No. 721432 (CarBon), and by the European Research Council (ERC) Advanced Grant No. 788753 (ReCaP).

Open access funding provided by IReL.

## Conflict of Interest

The authors declare no conflict of interest.

## Author Contributions

C.I., L.B.F., J.E.D., J.P.G., and F.J.O'B.: conceptualization; C.I.: investigation; C.I., S.C., J.E.D., J.P.G., and F.J.O'B.: writing, reviewing, and editing; J.P.G. and F.J.O'B.: funding acquisition. All authors have read and agreed to the published version of the manuscript.

## Data Availability Statement

The data that support the findings of this study are available from the corresponding author upon reasonable request.

## Keywords

biomimetic scaffold, cartilage repair, chondrogenesis, gene therapy, hypertrophic cartilage, microRNA-221

Received: December 1, 2022

Revised: January 23, 2023

Published online: May 3, 2023

- [1] T. Gonzalez-Fernandez, B. N. Sathy, C. Hobbs, G. M. Cuniffe, H. O. McCarthy, N. J. Dunne, V. Nicolosi, F. J. O'Brien, D. J. Kelly, *Acta Biomater.* **2017**, *55*, 226.
- [2] F. J. O'Brien, *Mater. Today* **2011**, *14*, 88.
- [3] W. Wei, H. Dai, *Bioact. Mater.* **2021**, *6*, 4830.
- [4] C. Intini, M. Lemoine, T. Hodgkinson, S. Casey, J. P. Gleeson, F. J. O'Brien, *Biomater. Sci.* **2022**, *10*, 970.
- [5] C. Intini, T. Hodgkinson, S. M. Casey, J. P. Gleeson, F. J. O'Brien, *Bioengineering* **2022**, *9*, 232.
- [6] T. J. Levingstone, A. Matsiko, G. R. Dickson, F. J. O'Brien, J. P. Gleeson, *Acta Biomater.* **2014**, *10*, 1996.
- [7] T. J. Levingstone, A. Ramesh, R. T. Brady, P. A. J. Brama, C. Kearney, J. P. Gleeson, F. J. O'Brien, *Biomaterials* **2016**, *87*, 69.
- [8] A. R. Armiento, M. Alini, M. J. Stoddart, *Adv. Drug Delivery Rev.* **2019**, *146*, 289.
- [9] M. Gugjoo, Amarpal, G. Sharma, H. Aithal, P. Kinjavdekar, *Indian J. Med. Res.* **2016**, *144*, 339.
- [10] A. Colombini, C. Perucca Orfei, D. Kouroupis, E. Ragni, P. De Luca, M. Viganò, D. Correa, L. De Girolamo, *Cytotherapy* **2019**, *21*, 1179.
- [11] S. Chen, P. Fu, R. Cong, H. Wu, M. Pei, *Genes Dis.* **2015**, *2*, 76.
- [12] P. Occhetta, S. Pigeot, M. Rasponi, B. Dasen, A. Mehrkens, T. Ullrich, I. Kramer, S. Guth-Gundel, A. Barbero, I. Martin, *Proc. Natl. Acad. Sci. USA* **2018**, *115*, 4625.
- [13] R. M. Raftery, A. G. Gonzalez Vazquez, G. Chen, F. J. O'Brien, *Adv. Healthcare Mater.* **2020**, *9*, 1901827.
- [14] R. M. Raftery, I. Mencía Castaño, G. Chen, B. Cavanagh, B. Quinn, C. M. Curtin, S. A. Cryan, F. J. O'Brien, *Biomaterials* **2017**, *149*, 116.
- [15] R. M. Raftery, D. P. Walsh, L. Blokpoel Ferreras, I. Mencía Castaño, G. Chen, M. Lemoine, G. Osman, K. M. Shakesheff, J. E. Dixon, F. J. O'Brien, *Biomaterials* **2019**, *216*, 119277.
- [16] C. M. Curtin, E. G. Tierney, K. M. Morsorley, S.-A. Cryan, G. P. Duffy, F. J. O'Brien, *Adv. Healthcare Mater.* **2015**, *4*, 223.
- [17] L. S. Costard, D. C. Kelly, R. N. Power, C. Hobbs, S. Jaskaniec, V. Nicolosi, B. L. Cavanagh, C. M. Curtin, F. J. O'Brien, *Pharmaceutics* **2020**, *12*, 1219.
- [18] I. Mencía Castaño, C. M. Curtin, G. P. Duffy, F. J. O'Brien, *Sci. Rep.* **2016**, *6*, 27941.
- [19] T. Gonzalez-Fernandez, D. J. Kelly, F. J. O'Brien, *Adv. Ther.* **2018**, *1*, 1800038.
- [20] E. G. Tierney, K. Morsorley, C. L. Hastings, S.-A. Cryan, T. O'Brien, M. J. Murphy, F. P. Barry, F. J. O'Brien, G. P. Duffy, *J. Controlled Release* **2013**, *165*, 173.
- [21] J. E. Dixon, G. Osman, G. E. Morris, H. Markides, M. Rotherham, Z. Bayoussef, A. J. El Haj, C. Denning, K. M. Shakesheff, *Proc. Natl. Acad. Sci. USA* **2016**, *113*, E291.
- [22] L. Thiagarajan, H. Al-D. M. Abu-Awwad, J. E. Dixon, *Stem Cells Transl. Med.* **2017**, *6*, 2146.
- [23] H. M. Eltaher, J. Yang, K. M. Shakesheff, J. E. Dixon, *Acta Biomater.* **2016**, *41*, 181.
- [24] C.-Y. Jiao, D. Delaroche, F. Burlina, I. D. Alves, G. Chassaing, S. Sagan, *J. Biol. Chem.* **2009**, *284*, 33957.
- [25] E. Van Rooij, A. L. Purcell, A. A. Levin, *Circ. Res.* **2012**, *110*, 496.
- [26] Q. Leng, L. Chen, Y. Lv, *Theranostics* **2020**, *10*, 3190.
- [27] C. M. Curtin, I. M. Castaño, F. J. O'Brien, *Adv. Healthcare Mater.* **2018**, *7*, 1700695.
- [28] K. Chen, N. Rajewsky, *Nat. Rev. Genet.* **2007**, *8*, 93.
- [29] E. G. Tierney, G. P. Duffy, S.-A. Cryan, C. M. Curtin, F. J. O'Brien, *Organogenesis* **2013**, *9*, 22.
- [30] N. Z. Laird, T. M. Aciri, K. Tingle, A. K. Salem, *Adv. Drug Delivery Rev.* **2021**, *174*, 613.
- [31] M. A. Arriaga, M.-H. Ding, A. S. Gutierrez, S. A. Chew, *Biotechnol. J.* **2019**, *14*, 1900084.
- [32] A. Lolli, E. Lambertini, L. Penolazzi, M. Angelozzi, C. Morganti, T. Franceschetti, S. Pelucchi, R. Gambari, R. Piva, *Stem Cell Rev. Rep.* **2014**, *10*, 841.
- [33] A. Lolli, R. Narcisi, E. Lambertini, L. Penolazzi, M. Angelozzi, N. Kops, S. Gasparini, G. J. V. M. Van Osch, R. Piva, *Stem Cells* **2016**, *34*, 1801.
- [34] D. Kim, J. Song, E.-J. Jin, *J. Biol. Chem.* **2010**, *285*, 26900.
- [35] A. Lolli, K. Sivasubramanian, M. L. Vainieri, J. Oieni, N. Kops, A. Yayon, G. J. V. M. Van Osch, *J. Controlled Release* **2019**, *309*, 220.
- [36] D. Napierala, K. Sam, R. Morello, Q. Zheng, E. Munivez, R. A. Shivasani, B. Lee, *Hum. Mol. Genet.* **2008**, *17*, 2244.
- [37] A. González-Vázquez, R. M. Raftery, S. Günbay, G. Chen, D. J. Murray, F. J. O'Brien, *Biomaterials* **2021**, *268*, 120540.
- [38] M. G. Haugh, C. M. Murphy, F. J. O'Brien, *Tissue Eng., Part C* **2010**, *16*, 887.

- [39] P. Singh, K. B. Marcu, M. B. Goldring, M. Otero, *Ann. N. Y. Acad. Sci.* **2019**, 1442, 17.
- [40] S. K. Bulstra, J. Drukker, R. Kuijjer, W. A. Buurman, A. J. V. D. Linden, *Biotech. Histochem.* **1993**, 68, 20.
- [41] C. a Knuth, E. Andres Sastre, N. Fahy, J. Witte-Bouma, Y. Ridwan, E. m Strabbing, M. j Koudstaal, J. Van De Peppel, E. Wolvius, R. Narcisi, E. Farrell, *Eur. Cells Mater.* **2019**, 38, 106.
- [42] M. B. Goldring, *Ther. Adv. Musculoskeletal Dis.* **2012**, 4, 269.
- [43] M. Wuelling, F. J. Kaiser, L. A. Buelens, D. Braunholz, R. A. Shivdasani, R. Depping, A. Vortkamp, *Dev. Biol.* **2009**, 328, 40.
- [44] Y. Chen, T. Gridley, *Biochem. Biophys. Res. Commun.* **2013**, 435, 356.
- [45] I. M. Castaño, C. M. Curtin, G. Shaw, J. Mary Murphy, G. P. Duffy, F. J. O'Brien, *J. Controlled Release* **2015**, 200, 42.
- [46] G. M. Cunniffe, G. R. Dickson, S. Partap, K. T. Stanton, F. J. O'Brien, *J. Mater. Sci.: Mater. Med.* **2010**, 21, 2293.
- [47] R. Sridharan, K. J. Genoud, D. J. Kelly, F. J. O'Brien, *ACS Appl. Bio Mater.* **2020**, 3, 7562.
- [48] Y. Song, H. Wu, Y. i Gao, J. Li, K. Lin, B. Liu, X. Lei, P. Cheng, S. Zhang, Y. Wang, J. Sun, L. Bi, G. Pei, *ACS Appl. Mater. Interfaces* **2020**, 12, 16058.
- [49] X. Lei, J. Gao, F. Xing, Y. Zhang, Y. Ma, G. Zhang, *Regener. Biomater.* **2019**, 6, 361.